NOTATION

a = radius of active particles, cm
C = reactant concentration inside diluted pellet, moles/cm^3
C_o = reactant concentration at external surface of pellet, moles/cm^3
$C_{\bar{z}}$ = reactant concentration at poison front, moles/cm^3
Cp_o = poison precursor concentration at external surface of pellet, moles/cm^3
CW_i = saturation poison capacity in support i, moles/cm^3
CW_e = saturation poison capacity in diluted pellet, moles/cm^3
D_i = reactant effective diffusivity in support i, cm^2/sec
D_e = reactant effective diffusivity in diluted pellet, cm^2/sec.
Dp_i = poison precursor effective diffusivity in support i, cm^2/sec.
Dp_e = poison precursor effective diffusivity in diluted pellet, cm^2/sec.
f = fraction of volume occupied by active particles
h_o = Thiele modulus of undiluted pellet of same dimensions
k = reaction rate constant, sec^{-1}
L = half-thickness of catalyst pellet, cm
r = radial distance inside active particle, cm
R = reaction rate in diluted pellet, moles/cm^3-sec.
R_o = initial reaction rate in undiluted pellet, moles/cm^3-sec.
t = time, sec.
u = reactant concentration inside active particle, moles/cm^3
u_o = reactant concentration at surface of active particle, moles/cm^3
z = distance inside pellet, cm
$\bar{z}$ = depth of poison penetration, cm

Greek Letters

Δ = fractional depth of poison penetration, $\bar{z}/L$
ξ = effectiveness factor
τ = dimensionless time

Subscripts

1 = identify the inert support or diluent
2 = identify the support containing active material

LITERATURE CITED

Aris, R., "On Shape Factors for Irregular Particles. I. The Steady State Problem. Diffusion and Reaction," *Chem. Eng. Sci.*, 6, 262 (1957).

Balder, J. R., and E. E. Petersen, "Poisoning Studies in a Single Pellet Reactor," *Chem. Eng. Sci.*, **23**, 1287 (1968).

Becker, E. R., and J. Wei, "Nonuniform Distribution of Catalysts on Supports," I. "Bimolecular Langmuir Reactions," *J. Catal.*, 46, 365 (1977). II. "First Order Reactions with Poisoning," *J. Catal.*, 46, 372 (1977).

Carberry, J. J., "Chemical and Catalytic Reaction Engineering," McGraw-Hill, New York, N.Y., 1976.

Carberry, J. J. and R. L. Gorring, "Time Dependent Pore Mouth Poisoning of Catalysts," *J. Catal.*, **5**, 529 (1966).

DeLancey, G. B., "Optimum Density and Composition for Catalytic Pellets," *Chem. Eng. Sci.*, **29**, 1391 (1974).

Hegedus, L. L., and J. C. Cavendish, "Intrapellet Diffusivities from Integral Reactor Models and Experiments," *Ind. Eng. Chem. Fundamentals*, **16**, 356 (1976).

Hegedus, L. L., and J. C. Summers, "Improving the Poison Resistance of Supported Catalysts," *J. Catal.*, **48**, 345 (1977).

McArthur, D. P., "Deposition and Distribution of Lead, Phosphorus, Calcium, Zinc, and Sulfur Poisons on Automobile Exhaust NO_x Catalysts," from *Catalysts for the Control of Automotive Pollutants*, Advances in Chemistry Series, No. 143, ACS, 1975.

Polomski, R. E., and E. E. Wolf, "Deactivation of a Composite Automobile Catalyst Pellet, II. Bimolecular Langmuir Reaction," *J. Catal.*, **52**, 272 (1978).

Ruckenstein, E., "The Effectiveness of Diluted Porous Catalysts," *AIChE J.*, **16**, 151 (1970).

Wheeler, A., "Reaction Rates and Selectivity in Catalyst Pores," *Adv. Catalysis*, 3, 250 (1951).

Wolf, E. E., "Activity and Lifetime of a Composite Automobile Catalyst Pellet," *J. Catal.*, **47**, 85 (1977).

Manuscript received September 19, 1978; revision received July 3, and accepted July 10, 1979.

The Co-current Reactor-Heat Exchanger

A reactor of four crossflow monolithic blocks is used to approximate a cocurrent and a countercurrent reactor-heat exchanger. Essentially isothermal reaction pass profiles are produced by flowing the coolant and reactant streams cocurrent to each other according to the criteria set down in Part I of this paper. A multiplicity of steady states is shown to exist for the autothermal countercurrent mode, but not for the autothermal cocurrent mode, under identical conditions.

THOMAS F. DEGNAN

and

JAMES WEI

Chemical Engineering Department
University of Delaware
Newark, Delaware 19711

Part II. Experimental Results

SCOPE

Four crossflow monolith blocks are used to carry out an oxidation reaction in which heat is simultaneously generated and transferred to a coolant stream. The crossflow design is of particular interest because of its high heat transfer area-to-volume ratio.

Two cases are considered. In one, cylindrical catalyst pellets fill the volume through which the reactant stream flows. In the second case, a similar catalyst is coated on the walls of the reaction pass. The remaining monolith volume is comprised of coolant channels that run perpendicular to the reaction pass.

T. Degnan is with Minnesota Mining and Manufacturing Co., 3M Center, St. Paul, Minn. 55101. J. Wei is with Massachusetts Institute of Technology, Department of Chemical Engineering, Cambridge, Mass. 02139.

By feeding the coolant and reactant streams into the same crossflow block, a good approximation to a cocurrent reactor-heat exchanger is obtained over the length of the four blocks. Inlet conditions obtained from the design equations derived in Part I were used to determine the necessary conditions for isothermality, and to produce a relatively flat reaction pass temperature profile.

The four-block reactor-heat exchanger can be converted into either the autothermal cocurrent or autothermal countercurrent mode by first flowing the stream through the coolant pass and then through the reaction pass. Comparison of the stability behavior of the autothermal countercurrent and cocurrent modes is thus achieved in the same reactor.

CONCLUSIONS AND SIGNIFICANCE

A first-order irreversible oxidation reaction has been carried out in a series of four crossflow monolith blocks. The crossflow monoliths have heat transfer area-to-volume ratios on the order of 25 cm^{-1} to 50 cm^{-1}, and consequently provide more heat transfer per volume than conventional bundles of 5 cm diameter tubes in boiling medium.

By running this monolithic reactor-heat exchanger (MRHE) in a pseudo-cocurrent mode (i.e., feeding both reaction and cooling streams parallel into the same crossflow block), nearly isothermal profiles are attained in the reaction pass. The operating conditions necessary to achieve this result are obtained from theoretical equations derived in Part I of this paper.

The predicted dual steady states were obtained when the MRHEs were operated in the countercurrent mode, in the region of operating conditions calculated to produce a multiplicity of steady states. Transition time from the lower to upper steady state is 12.2 hours, while the return time from the upper to the lower steady state is 9.5 hours. Under identical operating conditions, the autothermal cocurrent reactor heat exchanger shows no steady state multiplicity.

The theoretical development of the cocurrent reactor-heat exchanger is presented in Part I of this paper. In Part II, we report the experimental results obtained at a bench-scale prototype reactor-heat exchanger.

This reactor consists of a series of four crossflow monoliths arranged in series, so as to simulate either a cocurrent or a countercurrent configuration. These crossflows are made of cordierite, and have sinusoidal-shaped ducts. A schematic of one of these monoliths is shown in Figure 1.

Two cases are considered. In the first, cylindrical alumina pellets with deposited catalyst fill the monolith volume, through which a reactant stream flows. In the second case, a similar catalyst is coated on the sinusoidal and flat surfaces of this same reaction volume. The remaining monolith volume, consisting of the ducts which run perpendicular to the reaction pass, is used for the coolant medium in both cases.

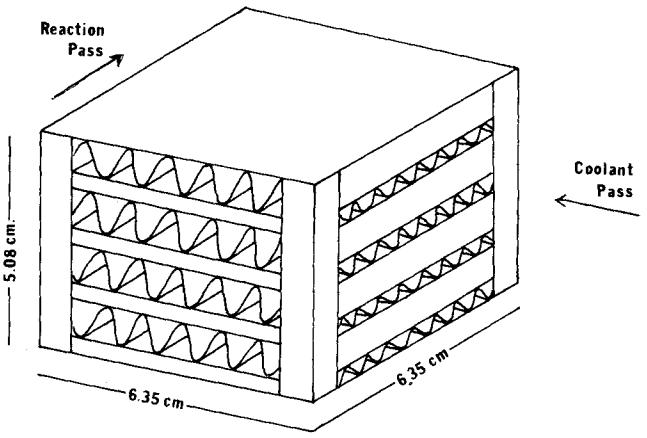

Figure 1. Cross flow monolith: The larger pass is for pellets and the reaction stream.

TABLE 1. DIMENSIONS OF MONOLITH BLOCKS

	Pellet-filled monoliths		Coated wall monoliths
	Reactant pass	Coolant pass	Either pass
Height of corrugation, h	0.8 cm	0.3125 cm	0.1984 cm
Width of pass, w	5.08 cm	5.08 cm	5.08 cm
Heat transfer area, A	556.16 cm^2	437.50 cm^2	1,346.5 cm^2
Open volume, V	76.227 cm^3	28.42 cm^3	46.24 cm^3
Open face area, A^c	15.0 cm^2	5.6 cm^2	6.8 cm^2
Frontal area, A_f	26.6 cm^2	26.6 cm^2	26.6 cm^2
Hydraulic radius	0.137 cm	0.065 cm	0.034 cm
Ratio of total heat transfer area of pass to total volume of pass, ψ	7.3 cm^{-1}	15.39 cm^{-1}	29.13 cm^{-1}
Ratio of total heat transfer area of pass to total volume of monolith, ω	4.5 cm^{-1}	3.8 cm^{-1}	7.76 cm^{-1}
Surface area of sinusoids	417.25 cm^2	285.40 cm^2	805.2 cm^2
Ratio of free flow area to frontal area, σ	0.5639	0.2102	0.267

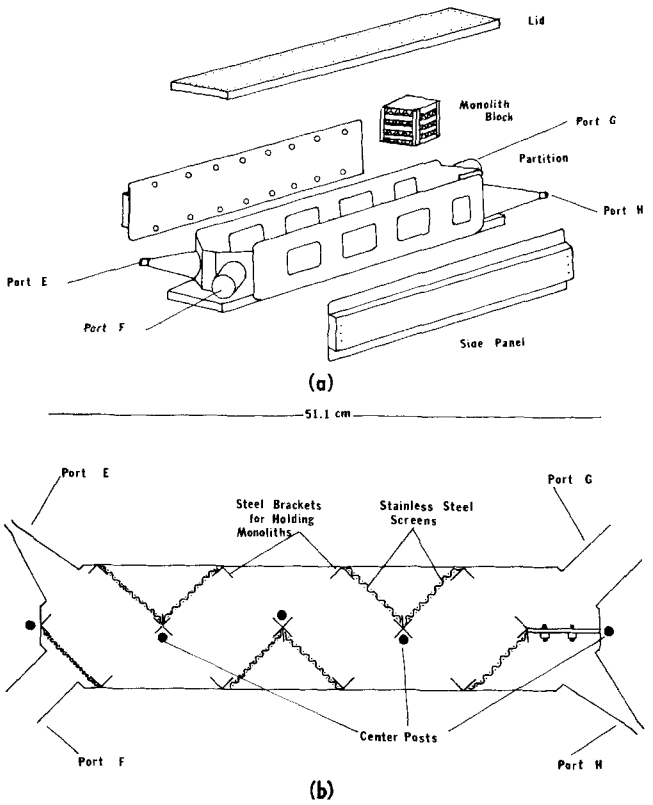

Figure 2. Reactor before assembly *(a)* and top view of reactor *(b)*.

The advantage of the crossflows monoliths lies in its large heat transfer area-to-volume ratio, giving the potential of transferring more heat over shorter flow lengths. Table 1 lists the dimensions of the monoliths used here. In a comparable reactor-heat exchanger consisting of either a single or a multiplicity of tubes, each tube would require an inner diameter of 0.14 cm to have an equivalent area-to-volume ratio.

EXPERIMENTAL

For the pelleted case, copper chrome (1.44% Cu, 0.97% Cr) "Aero Ban" catalyst provided by American Cyanamid Co. was used as the oxidation catalyst for the reaction $CO + \frac{1}{2}O_2 \rightarrow CO_2$. This is a highly exothermic reaction ($-\Delta H = 67.22$ kcal/kg mole or 0.2813 kJ/kg mole) that has been shown to be approximately first order and irreversible (Yu-Yao 1975, Harned 1971, Hertl and Farrauto 1973). This pelleted catalyst was metered into each of the sinusoidal ducts of the reaction pass of the four monoliths. A one-centimeter layer of quartz chips preceded and followed each length of catalyst so that the reaction was confined to the heat transfer section of the crossflow (see Figure 1). Stainless steel screens affixed to the faces of the reaction side contained the pellets.

In the catalyst-coated scheme, a catalyst of approximately the same copper-chrome composition as that in the outer layer of the cylindrical pellets was used to impregnate the walls of the reaction pass in each of the four monoliths.

The four cordierite monoliths are positioned in a box-like steel manifold as shown in Figures 2a and 2b. Sixty-one thermocouples are used to measure the temperatures within the reactor-heat exchanger. Five chrome-alumel thermocouples are situated in the reaction pass and four in the coolant pass of each monolith, to monitor the two-dimensional temperature profile characteristics of crossflows (Nusselt 1927). At least two thermocouples are positioned in each of the triangular chambers between the monoliths. Thermocouple potentials are recorded on a multipoint digital voltmeter that printed the data in digital form on a paper tape.

Five modes of operation were attempted in the prototype. To simulate an adiabatic reactor, ports E and G were sealed and a preheated stream of air containing CO fed into port H. Simple cocurrent and countercurrent flow of reactant and coolant streams are approximated by feeding the CO containing stream at port H and feeding a stream of ambient temperature

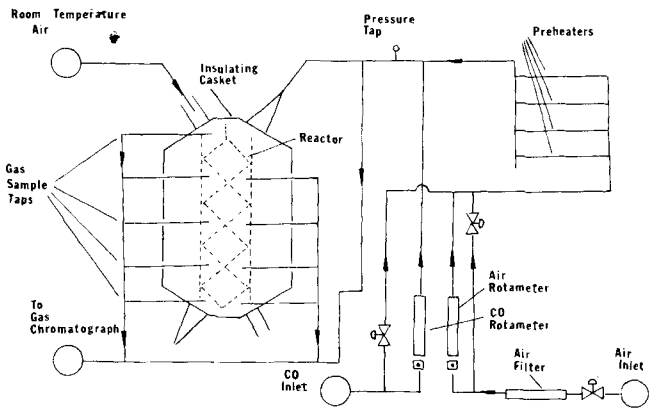

Figure 3. Reaction system.

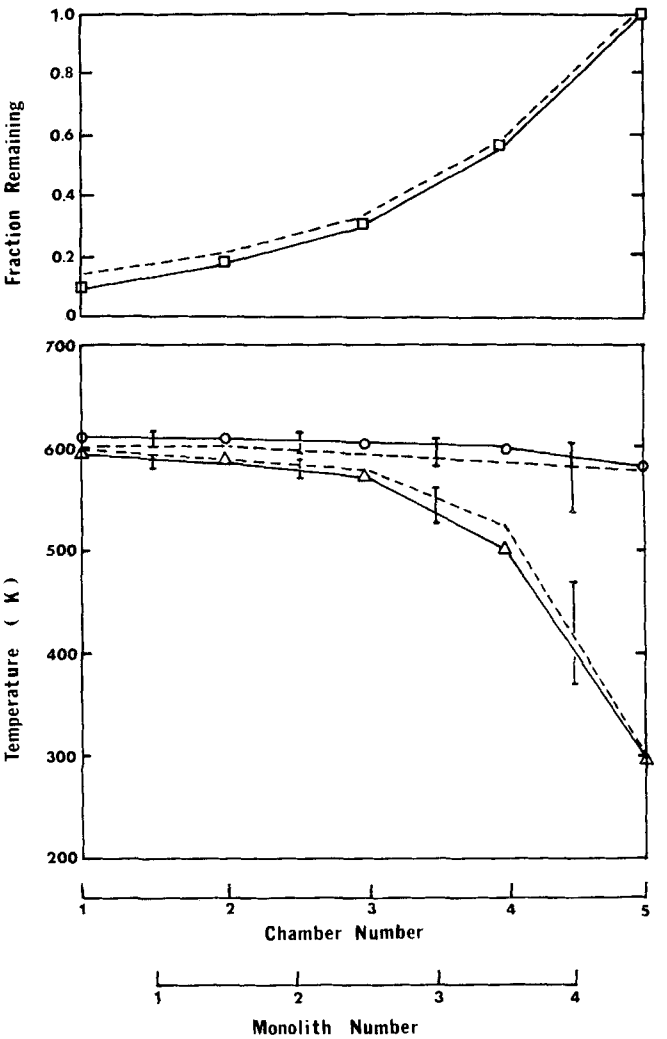

Figure 4. An autothermal cocurrent run in pellet-filled monoliths. For data from entrance, exit and triangular chambers: □ fraction CO remaining, ○ reactant temperature, △ coolant temperature. For data from probes inside monoliths: I showing range of temperatures measured. Theoretical predictions from a cell model are shown by broken lines.

(23°C = 74°F) either to port G or to port E. Finally, autothermal cocurrent and countercurrent modes are approximated by feeding the stream into port E and leaving port G. In the autothermal cocurrent mode, an insulated stainless steel flex hose connected port G and port F, while in the autothermal countercurrent mode the insulated barrier is removed and ports G and H are sealed.

Segments of stainless steel tubing, 17 cm long, are welded into holes drilled in the manifold wall at the center of each of the ten chambers for use as gas sample ports (shown in Figure 3). Sample analysis was performed with a gas chromatograph. Six nichrome wound heaters controlled by variacs heated the inlet stream. Calibrated rotameters ind cated the CO and air flow rates. The entire manifold is surrounded by 15 cm of vermiculite insulation.

RESULTS

Kinetics of the American Cyanamid pelleted catalyst were characterized by an integral reactor immersed in a sandbath, and an experimental analysis of the heat transfer capability was performed. The necessary operating conditions to produce a nearly isothermal autothermal reaction pass profile are

$$NTU^c = \beta \exp(-\alpha/\theta^l{}_o) \tag{1}$$

$$Y = \exp(-\xi NTU^c) \tag{2}$$

$$(\theta_o{}^R - \theta_o{}^c) = NTU^c/NTU^R \tag{3}$$

These equations were derived previously (Degnan and Wei 1978). For one run, the experimental results of conversion and the temperatures of the reactant and coolant are shown in Figure 4. Theoretical predictions from a cell model, using the actual inlet conditions, are shown by the broken lines. Vertical lines passing through each of the data points of the profile show the maximum and minimum temperatures measured in the monoliths and chambers. The data points represent the averaged temperatures. The operating conditions of this run are shown in Table 2.

A crossflow monolith is an imperfect approximation of a true cocurrent reactor, especially when the reaction rate is high. The largest span between maximum and minimum temperatures within a monolith is observed in the first monolith where much of the conversion and heat transfer take place. In each of the monoliths, the reaction stream entering the catalyst duct closest to the coolant gas inlet is overcooled, since this stream is experiencing the low coolant inlet temperature along the length of the duct.

An analogous case is a small diameter catalyst-filled tube immersed in a low temperature medium. In the catalyst-containing duct farthest from the entrance of the coolant stream, much less heat is transferred across the wall separating the reactant and coolant passes, be-

Table 2. Comparison Between Experimental and Calculated Values Predicted from Model for Run Shown in Figure 4

	Observed	Specified in model
Coolant inlet temperature	24°C (75°F)	24°C (75°F)
Reaction pass inlet temperature	304.4°C (580°F)	304.4°C (580°F)
% CO in reaction pass inlet stream	3.0	3.0
Composition of coolant stream	Air	Air
ΔT_{AD}	232°C (420°F)	232°C (420°F)
$ACT = \exp(-\alpha/\theta_0{}^R)$	1.735	1.735
$DT = (\theta_0{}^R - \theta_0{}^c)$	1.21	1.21
Reactant pass inlet flow rate	253.1 gm mole/hr	253.1 gm mole/hr
	Observed	**Predicted**
Conversion	0.125	0.122
Max./Min. reactant pass: (°C)		
Block 1	327/260	326/262
Block 2	331/299	329/302
Block 3	335/317	333/320
Block 4	334/323	332/325
Max./Min. coolant pass: (°C)		
Block 1	193/94	199/99
Block 2	287/249	293/253
Block 3	316/293	319/295
Block 4	319/306	321/307
NTU^R	2.4	2.04
NTU^c	2.4	1.735
Coolant pass inlet flow rate	367.3 gm mole/hr	588 gm mole/hr

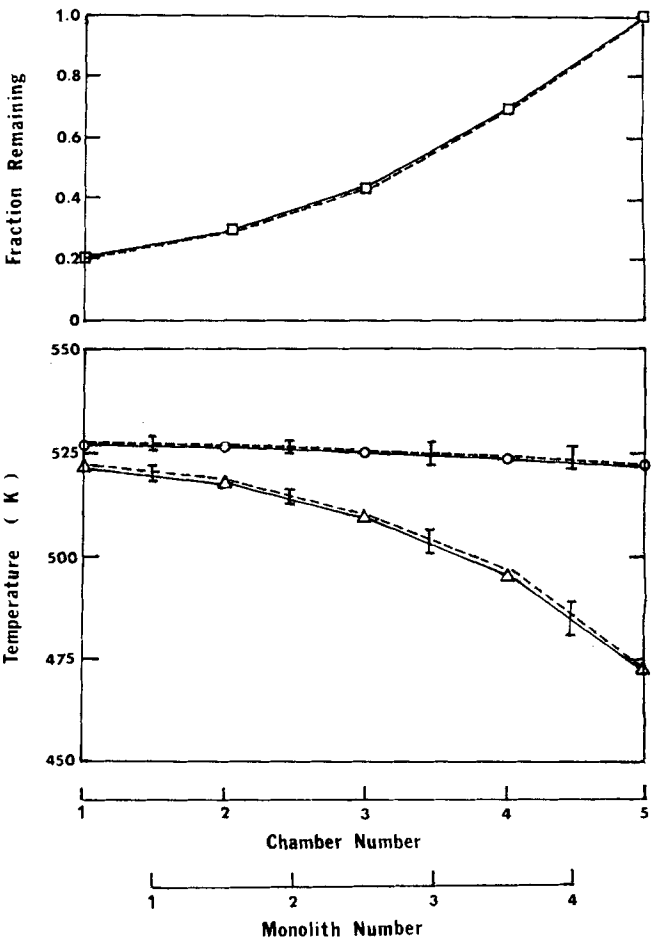

Figure 5. Another autothermal cocurrent, run in pellet-filled monoliths with less reaction in first block (notation as in Figure 4).

Table 3. Comparison Between Experimental and Calculated Values Predicted from Model for Run Shown in Figure 5

	Observed	Specified in model
Coolant pass inlet temperature	200°C (390°F)	200°C (390°F)
Reactant pass inlet temperature	225°C (480°F)	225°C (480°F)
% CO in reactant pass inlet stream	2.0	2.0
Composition of coolant stream	Air	Air
ΔT_{AD}	156°C (280°F)	156°C (280°F)
$ACT = \beta\exp(-\alpha/\theta_0^R)$	2.0	2.0
$DT = (\theta_0^R - \theta_0^c)$	0.358	0.358
Reaction pass inlet flow rate	43.1 gm mole/hr	43.1 gm mole/hr
	Observed	**Predicted**
Conversion	0.192	0.19
Max./Min. temp. reaction pass: (°C)		
Block 1	254/246	256/243
Block 2	254/248	256/247
Block 3	253/249	256/248
Block 4	253/248	256/247
Max./Min. temp. coolant pass: (°C)		
Block 1	216/210	220/207
Block 2	233/229	236/227
Block 3	243/239	245/237
Block 4	247/244	248/243
NTU^R	5.50	5.53
NTU^c	2.0	1.966
Coolant pass inlet flow rate	236 gm mole/hr	250.5 gm mole/hr

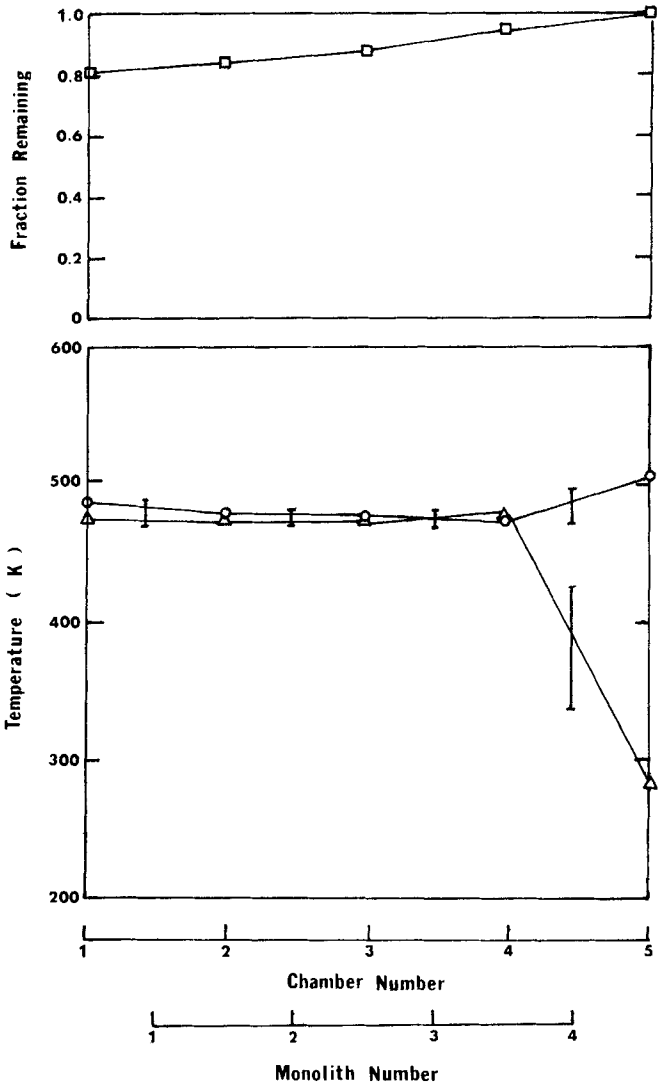

Figure 6. An autothermal cocurrent, run in wall-coated monoliths (notation as in Figure 4).

cause the thermal driving force is reduced. The maximum temperature in the monolith nearly always occurs near the point where both streams leave the crossflow.

Nevertheless, the observed difference between the maximum and minimum temperatures in the reaction pass is much less than what is predicted by theory. Conduction within the small crossflowing monoliths tends to reduce the heat exchange efficiency, by making the temperature more uniform across the block. Kays and London (1964) have shown that conduction in any crossflow is

Table 4. Operating Conditions for Runs Shown in Figures 6, 8, and 9

	Figure 6	Figure 8	Figure 9
Inlet composition of coolant stream	2.3% CO	air	2.3% CO
Inlet composition of reactant stream	2.3% CO	4.56%	2.3% CO
Inlet temperature of coolant stream	various	24°C (75°F)	various
Inlet temperature of reactant stream	various	249°C (481°F)	various
Flow velocity of coolant stream	364 gm mole/hr	53.6 gm mole/hr	364 gm mole/hr
Flow velocity of reactant stream	364 gm mole/hr	364 gm mole/hr	362 gm mole/hr
k_e eff	11,920 sec^{-1}	*11,920 sec^{-1}	11,920 sec^{-1}
E/R	6,300	*6,300	6,300
ΔT_{AD}	179°C (322°F)	354°C (638°F)	179°C (322°F)
τ	0.0655 sec	0.0476 sec	0.0655 sec
Pressure	1 atm	1 atm	1 atm

* Assumed values on catalyst coated monoliths.

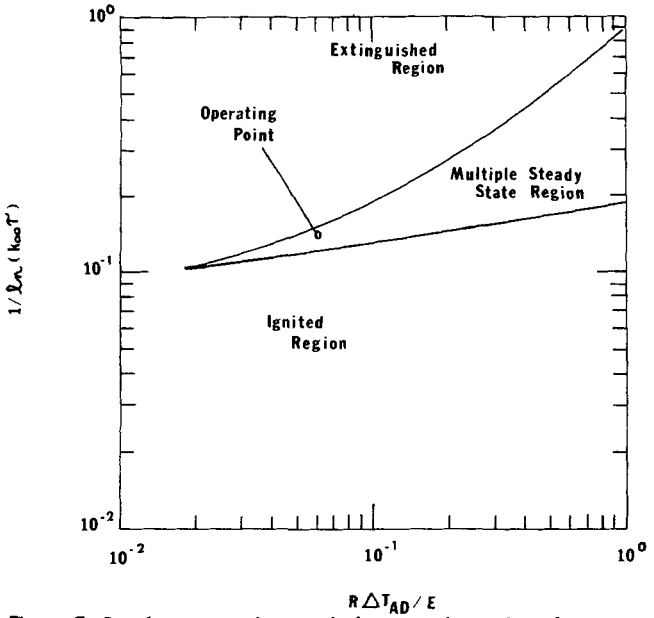

Figure 7. Steady-state regions and the operating point of one experiment in autothermal countercurrent operation.

of the order

$$q = kA_k \frac{\delta T}{l} \tag{4}$$

where δT is the temperature difference between the hot and cold streams, l is the length of the pass, A_k is the cross sectional area for longitudinal conduction, and k is the thermal conductivity of the material. Conduction is therefore particularly severe in small crossflows where large thermal gradients appear, such as the catalyst-filled crossflows considered here. Moreover, while the effect of conduction upon the two-dimensional profile of a small crossflow is significant, this effect is amplified in the case of simultaneous reaction and heat transfer. This is so due to the exponential dependence of the reaction rate and heat generation upon the temperature.

Comparison between the values predicted by the theory for cocurrent reactor-heat exchangers and values computed from experimental measurements on the monoliths is shown in Table 2. The slight disparity between calculated and experimental values can be attributed to the crossflow nature incurred by the large amount of conversion in the first monolith.

Figure 5 shows another autothermal cocurrent run with less conversion on the first block, with nearly flat reaction

Table 5. Temperature and Conversion Measurements for Stability Diagrams

Coolant inlet temperature °F (°C)	Coolant exit temperature °F (°C)		Conversion 1-C/CO	
	Countercurrent	Cocurrent	Countercurrent	Cocurrent
267.5 (130.8)	237.9 (114.4)		0.098	
280.0 (137.8)	245.0 (118.3)		0.121	
290 (143.3)	253.5 (123.1)		0.152	
300 (148.9)		298 (147.8)		0.023
302 (point 4) (150.0)	262.5 (128.1)		0.176	
302 (point 21) (150.0)	262.5 (128.1)		0.183	
307.5* (153.1)	483.0 (250.6)		0 682	
307.6 (153.1)	270.0 (132.2)		0.193	
312.5* (155.8)	487.0 (252.8)		0.692	
317* (158.3)	491.0 (255.0)		0.702	
320 (160.0)	285.0 (140.6)	327 (163.9)	0.201	0.036
325* (162.8)	496.5 (258.1)		0.729	
328.6* (164.8)	500.5 (260.3)		0.731	
330 (165.6)		339 (170.6)		0.041
335 (168.3)	300 (148.9)		0.205	
342 (172.2)	312 (155.6)	357 (180.6)	0.224	0.174
342* (172.2)	515.0 (268.3)		0.762	
347 (175.0)	317.5 (158.6)		0.241	
348* (175.6)	521 (271.7)		0.770	
370 (187.8)		401 (205.0)		0.257
375* (190.6)	555 (290.6)		0.793	
380 (193.3)		421 (216.1)		0.354
387.5* (197.5)	573 (301.7)		0.821	
396 (202.2)		447 (230.6)		0.393
400* (204.4)	587.5 (308.6)		0.845	
408 (208.9)		462 (238.9)		0.437
420 (215.6)		480 (248.9)		0.454
431 (221.7)	639 (337.2)		0.886	
474 (245.6)		538 (281.1)		0.503
514 (267.8)		580 (304.4)		0.560
536 (280.0)		680 (320.0)		0.570
557 (291.7)		643 (339.4)		0.620
586 (307.8)		690 (365.6)		0.695
600 (315.6)		715 (379.4)		0.712
700 (371.1)		831 (443.9)		0.753
797 (425.0)		929 (498.3)		0.797

* Denotes position on ignited branch of countercurrent case.

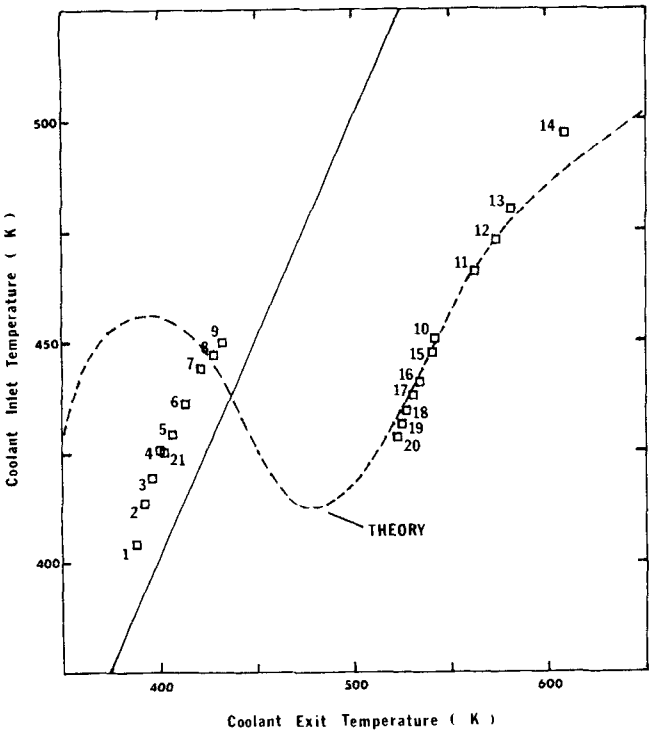

Figure 8. Data from a series of autothermal countercurrent experiments in pellet-filled reactor. Solid line indicates the adiabatic extinguished state when there is no heat loss to the surroundings. Dotted line shows theory based on heat loss to surroundings.

pass temperature profile. In this case, the reaction is spread more evenly over the four blocks. The result is a reduced difference among the temperatures measured in each monolith block, and a reduced difference between the predicted and calculated values describing the system as shown in Table 3.

COATED MONOLITH

Attempts to obtain a flat reaction pass temperature profile in monoliths coated with a similar catalyst composition produced the profile shown in Figure 6. Operating conditions are given in Table 4. Comparison between experimentally measured and theoretical values from isothermality theory was good when the estimated catalyst loading is 65% of that in the pellet-filled monoliths. The NTU^c value computed from the equation relating exit conversion to the coolant pass heat transfer parameters

$$(C/C_o)_{\text{exit}} = \exp(-NTU^c) \qquad (5)$$

was low when compared to the measured value. The implication is that the coolant in wall-coated monolith is more effective on the reaction side than in the pellet-filled monoliths. Depositing the catalyst on cordierite walls reduces the thermal mass of the system, decreases the catalytic surface area, and, most importantly, increases the heat transfer—since the gas film resistance on the reaction side no longer exists. Monoliths of smaller volume are necessary where the catalyst is deposited on the walls vs. pellet-filling, if the series of monoliths is to approximate a cocurrent reactor-heat exchanger.

STABILITY AND PARAMETRIC SENSITIVITY

Theory predicted that the four pellet-filled crossflow monoliths in series should exhibit multiple steady-state behavior when run in a counter-current autothermal mode

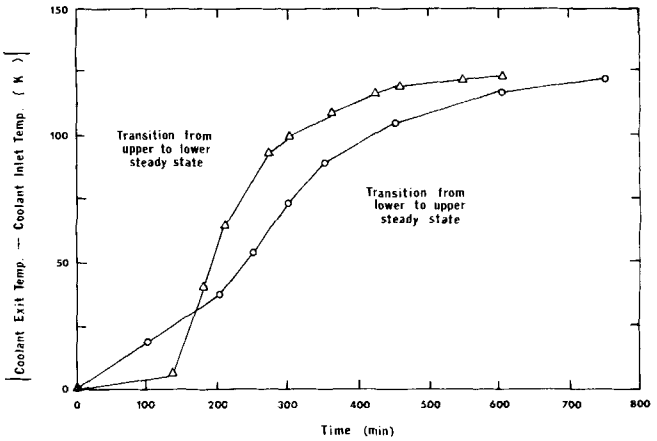

Figure 9. The time behavior of the transition between steady-states in autothermal countercurrent reactor.

for the range of values shown in Figure 7. These values are similar to the stability plot first proposed by Van Heerden (1958) for autothermic processes. The region above the upper curve of the wedge shown in the figure is the extinct region, where no reaction is occurring because "light off" has not yet taken place. Beneath the bottom line of the wedge and to the right of the point where the two curves of the wedge intersect, the reaction is ignited. Sandwiched between the two curves is the region of steady-state multiplicity, where the reaction may or may not have ignited. A more detailed explanation of this figure and its physical derivation can be found in the original article by Van Heerden (1959).

Multiple steady-states were studied in a series of autothermal countercurrent experiments in pellet-filled reactors. The operating conditions are given in Table 4, and the results in Figure 8. This series consists of setting the inlet temperature to a predetermined value and waiting for the MRHE to come to steady-state, and then repeating the procedure for many inlet temperatures. The dashed curve represents the cell model simulation using run

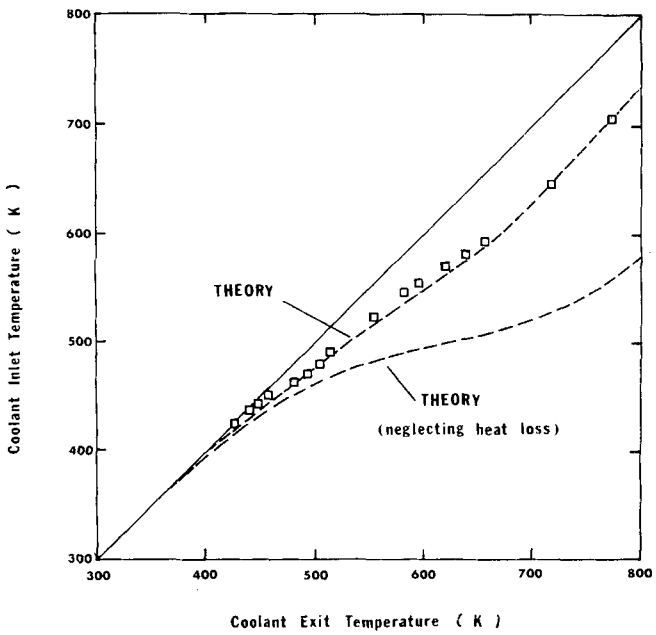

Figure 10. A series of autothermal cocurrent experiments, in pellet-filled reactor. Solid line is the extinguished state, where there is no heat loss to surroundings.

conditions. The data points are labeled numerically in the order in which they were observed. To obtain the temperature data on the low conversion branch of the stability curve, the inlet temperature To^c was increased gradually in a ramp-like manner from 138°C, allowing the MRHE to come to steady-state after each increment in the inlet temperature.

The time elapsed from incrementing To^c until the system reached steady-state varied in proportion to the size of the increment, but was normally 30 to 45 minutes. Temperature scans of nine thermocouples, representative of the temperature profile over the reactant and coolant passes, were made every five minutes throughout the entire analysis. When three successive readings showed no change, the reactor-heat exchanger was considered to be at steady-state.

At an inlet temperature to the coolant pass of 175.5°C (348°F) (point 9 in the figure) the reaction "lit off" and the temperature at the coolant exit gradually shifted to higher values (toward point 10 in the figure). The total time required to traverse the distance between the two steady-states was 12.2 hours. Once the reactor-heat exchanger attained an upper or ignited steady-state, the inlet temperature was increased further to elicit the shape of the upper steady-state. Upon reaching a value of 222°C (432°F), (point 14) To^c was decreased in a manner opposite that used in obtaining the lower steady-state data. At a coolant pass inlet temperature of 152°C (306°F) (point 20) the coolant exit temperature fell steadily until the extinguished steady-state branch was reached (point 21). The time elapsed in going from the ignited to the extinguished steady-state was 9.5 hours.

Heat loss from the reactor-heat exchanger can explain the difference in the rising and falling transit times between the two steady-state branches. When the reaction ignites at 175.5°C (347°F), it must fight an uphill battle against a system that is losing a large amount of heat (87.92 W/h or ~300 BTU/hr) to its surroundings. On the returning from the ignited to the extinguished states at a temperature of 152°C (306°F), the heat loss acts to push the reaction toward the lower steady-state. If the reactor-heat exchanger was insulated perfectly, the transition time would probably lie between 12.2 and 9.5 hours.

Figure 9 shows the time behavior of the difference between coolant inlet and exit temperatures for the two transitions. In going from the extinguished to the ignited steady-state, the reaction takes off rapidly, but slows down as it approaches the ignited steady-state branch. In contrast, the trip from the ignited to the extinguished steady-state starts slowly, accelerates rapidly between 150 and 200 minutes, then slows as it reaches the extinguished steady-state branch.

The reactor-heat exchanger was modified as described earlier to simulate an autothermal cocurrent reactor-heat exchanger. Conditions and procedures identical to those used in the autothermal countercurrent mode, when used for the autothermal cocurrent reactor-heat exchanger, produced the data shown in Figure 10. No steady-state multiplicity was observed in the 145°C (293°F) to 425°C (797°F) range. The dashed curve passing through the data is the theoretical prediction for the system obtained using a cell model that included a heat loss factor. Details of both runs are given in Table 5.

CONCLUSIONS

Theoretical results derived in the first part of this paper have been verified experimentally. In particular, a highly exothermic reaction can be operated isothermally by using a coolant stream that flows cocurrent, or approximately cocurrent, to the reactant stream. If a series of crossflow monoliths is used to approximate a cocurrent reactor-heat exchanger, each monolith must be small enough to minimize the temperature gradient within the first block in the reaction pass.

The multiplicity of steady-states in the monolithic reactor-heat exchanger has been experimentally demonstrated in an autothermal counter-current mode. Transition times from one steady-state branch to the other were on the order of 10 hours.

Theory and experiments agree that no multiple steady-states take place in running the reactor-heat exchanger in an autothermal cocurrent mode, under the same conditions at which multiplicity was observed in the countercurrent mode.

ACKNOWLEDGEMENT

The authors would like to thank the 3M Company for financial support and fabrication of the apparatus, and J. R. Johnson and W. C. Johnson for advice and encouragement.

NOTATION

A_k = cross-sectional area for longitudinal conduction
a = heat transfer area to flow volume ratio
C = concentration
C_p = heat capacity
E = activation energy
k = thermal conductivity of Cordierite
k_∞ = catalyst pre-exponential factor
l = length of the flow pass in monolith block
NTU = number of heat transfer units $= Ual/\rho C_p v$
q = heat flux due to thermal conductivity
R = gas constant
U = overall heat transfer coefficient
v = gas velocity in monolith duct
Y = fraction remaining

Greek Letters

α = catalyst activity factor $(=E/R\Delta T_{AD})$
β = reaction velocity parameter $(=k_\infty \tau^R)$
ΔH = heat of reaction
ΔT_{AD} = adiabatic temperature rise $(= -\Delta HCo/\rho C_p)$
δt = temperature difference between reactant and coolant passes
θ = dimensionless temperature $(=T/\Delta T_{AD})$
ξ = dimensionless temperature $(=x/L)$
ρ = density
τ = space time in monolith

Subscripts and Superscripts

c = coolant pass
o = initial value
R = reactant pass

LITERATURE CITED

Degnan, T. F., and J. Wei, "The Cocurrent Reactor-Heat Exchanger. Part I—Theory," *AIChE J.*, **25** (2), 338 (1979).

Hamed, J. L., "Analytical Evaluation of a Catalytic Converter System," Paper presented at Soc. Auto. Eng., SAE Paper 720520, Detroit, Michigan (May, 1973).

Hertl, W., and R. J. Farrauto, "Mechanism of Carbon Monoxide and Hydrocarbon Oxidation on Copper Chromite," *J. Catal.*, **28**, 352 (1973).

Nusselt, W., "Eine Neue Formel für der Warmedurchgang in Kreuzstrom," *Tech. Mech. Thermod.*, **1**, 417 (1930).

Van Heerden, C., "The Character of the Stationary State of Exothermic Processes," *Chem. Eng. Sci.*, **8**, 133 (1958).

Yu-Yao, Y. Y., "The Oxidation of CO and C_2H_2 Over Metal Oxides V. SO_2 Effects," *J. Catal.*, 39, 104 (1975).

Manuscript received January 4, 1978, and accepted January 3, 1979.